CHAPTER SEVENTY NINE

NEAR BOTTOM VELOCITIES IN WAVES WITH A CURRENT; ANALYTICAL AND NUMERICAL COMPUTATIONS

by
W.G.M. van Kesteren[1] and W.T. Bakker[2]

ABSTRACT
In this paper, starting from the Prandtl hypothesis a three-dimensional numerical bottom boundary layer model has been developed, which allows to calculate bottom friction by a combination of waves and currents. The model has been compared with two-dimensional analytical computations which gave similar results.
The bottom friction values found are comparable to the ones, found by Lundgren (1972), however in the most relevant cases somewhat less.
Furthermore in the two-dimensional case the model has been compared with measurements of Bakker and Van Doorn (1978).
With respect to the oscillatory motion, still some minor deviations occur between theory and measurements, due to deficiencies of the Prandtl theory.

1 Introduction

Investigation of the bottom boundary layer is primary of importance because it reveals the stirring mechanism of the sand in the surf zone. This is one of the most important factors, determining the sand transport in the surf zone and therefore coastal erosion and sedimentation.
Furthermore, the boundary layer determines the bottom friction and therefore the velocity of, for instance, the longshore current and the wave energy loss.

From the present paper may be expected:
- insight in the internal flow field, when waves and currents make an angle with each other;
- insight in the turbulent viscosity;
- a formula for bottom friction for waves and currents, making an angle with each other.

For this, the old, well-known Prandtl mixing-length theory is used.
From the data, presented by Bakker and Van Doorn (1978) it appears, that this theory overestimates the turbulent viscosity in the higher layers somewhat. Figure 1 shows a characteristic set of velocity profiles as measured by Van Doorn and as presented according to the Prandtl hypothesis. The general picture tallies, but the overshoot in reality is somewhat larger than theory predicts.

1) Project engineer, Delft Hydraulics Laboratory, the Netherlands (formerly: Delft University of Technology, the Netherlands).
2) Principal scientific officer Delft University of Technology; Scientific Coordinator Coastal Research of the Ministry of Transport and Public Works - Rijkswaterstaat.

2 Instantaneous velocity field

Assuming uniform flow in horizontal direction and the Prandtl/Von Karman hypothesis for the shear stress in Appendix A an equation is developed for the intrusion of the shear stress into the fluid:

$$\frac{\partial \underline{\tau}}{\partial t} = \underline{\underline{S}}\, \nu_t \frac{\partial^2 \underline{\tau}}{\partial z^2} \qquad (1) \qquad \text{wherein:} \quad \nu_t = \kappa z \sqrt{|\underline{\tau}|/\rho} \qquad (2)$$

Here τ stands for the shear stress with components (τ_x, τ_y), x and z are the horizontal and vertical coordinate respectively, t = the time, ρ = the specific density, ν_t the turbulent viscosity, κ = the Von Karman constant, and $\underline{\underline{S}}$ a second-order tensor, specified in Eq. (A9).

Eq. (1) is analogous to the famous diffusitivity equation, where the viscosity ν replaces the turbulent viscosity, and in which $\underline{\underline{S}}$ can be omitted. Tensor $\underline{\underline{S}}$ accounts for the difference in direction between $\partial \underline{\tau}/\partial t$ and $\partial^2 \underline{\tau}/\partial z^2$.

Furthermore, in appendix A an equation (A11), similar to (1) for the defect velocity $\underline{u}_d$ has been derived; the defect velocity is the difference $\underline{u}-\underline{U}$ between the velocity $\underline{U}$ far from the bottom and the local velocity $\underline{u}$ in the boundary layer (Fig. A1). This equation (A11) is solved numerically. Figure 1 gives a solution for the two-dimensional case, compared with data of Bakker and Van Doorn (1978). It shows, that the Prandtl hypothesis overestimates the turbulent viscosity in the higher layers somewhat. The general picture tallies, but the overshoot in reality is somewhat more than the theory predicts. Figure 2 shows the standard deviation (theory compared with measurements) as function of the height above the bottom. The figure demonstrates, that the present model is more accurate than the one, presented in 1978 (Bakker and Van Doorn), mainly because the upper boundary can be fulfilled without approximation.

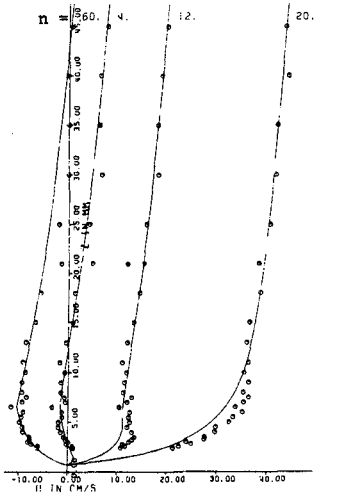

● measured profile at $t = \frac{n}{64}\,T$

—— theoretical profile (implicit computation)

Figure 1 Comparison theory (2 dim.) with experiment of Bakker and Van Doorn (1978)

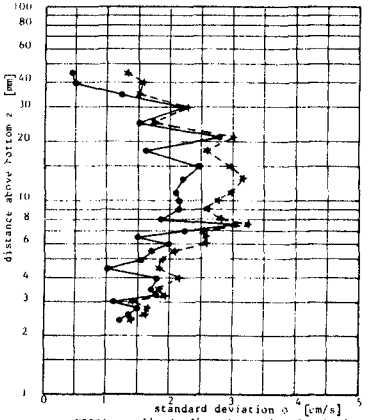

test V20RA: amplitude first harmonic of velocity just outside boundary layer: 24.3 cm/s
mean current velocity averaged over the height: 20 cm/s

—●— σ according to present numerical model

-●- σ according to numericel model oresented by Bakker and Van Doorn (1978)

Figure 2 Standard deviation between numerical theory and experiment of Bakker and Van Doorn (1978)

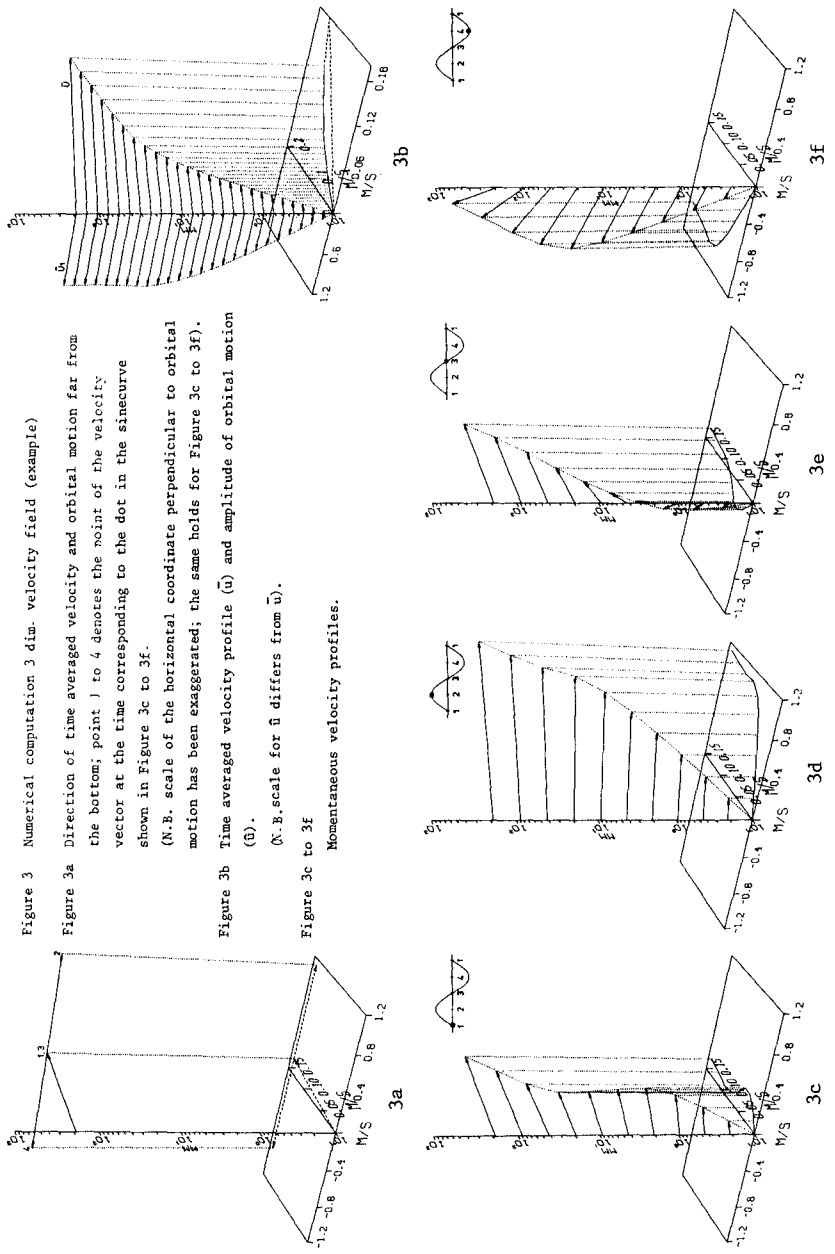

Figure 3 Numerical computation 3 dim. velocity field (example)

Figure 3a Direction of time averaged velocity and orbital motion far from the bottom; point 1 to 4 denotes the point of the velocity vector at the time corresponding to the dot in the sinecurve shown in Figure 3c to 3f.
(N.B. scale of the horizontal coordinate perpendicular to orbital motion has been exaggerated; the same holds for Figure 3c to 3f).

Figure 3b Time averaged velocity profile ($\bar{u}$) and amplitude of orbital motion ($\hat{u}$).
(N.B. scale for $\hat{u}$ differs from $\bar{u}$).

Figure 3c to 3f Momentaneous velocity profiles.

Figure 3 shows the solution in a three-dimensional case.
In Figure 3a the direction of the current far from the bottom is equal to the direction of the pressure gradient. The direction of the orbital motion is given by the points 1, 2 etc., representing the point of the current vector far from the bottom at successive times, 1/4 wave period apart. Figure 3c to 3f show these velocity profiles for 4 successive times. All the vectors are in a horizontal plane; the direction changes when going from upward to downward. In Figure 3b the resulting profile for the mean velocity and the amplitude of the first harmonic are shown. From this figure it appears that the direction of the mean velocity near the bottom differs considerable from the direction of the mean velocity outside the boundary layer, which asymptotically approaches the direction of the mean pressure gradient, or, which is the same, the mean shear stress. This effect should be taken into account in cases with for instance sandtransport near the bottom. The kink in the mean velocity profile will be treated in the next chapter.
Similar to the viscous boundary layer a unique relation can be expected in the turbulent case between horizontal velocity just outside the boundary layer and the shear stress acting on the bottom. However when the Prandtl hypothesis is used for determining the turbulent shear stresses in terms of the local velocity field it appears from analytical considerations (Appendix B) and numerical computations that only a unique relation can be obtained when the shear stress velocity p_b is used instead of the shear stress near the bottom τ_b.
The shear stress velocity $\underline{p}$ in the three dimensional case is defined as:

$$\underline{\tau} = \rho\, \underline{p}|\underline{p}| \tag{5}$$

The shear stress velocity can be expressed in terms of the local velocity field according to the Prandtl hypothesis (see Appendix B):

$$\underline{p} = \kappa z \frac{\partial \underline{u}}{\partial z} \tag{6}$$

The relation (5) has been treated more elaborate in Appendix B in order to make analytical computations of the instantaneous velocity field by linearizing Eq. (1) (see Appendix B) and of the time-averaged velocity field (see next chapter).
The amplitude of the first harmonic of the shear stress velocity $\hat{p}_b$ at the bottom is related to the amplitude of the first harmonic of the oscillation $\hat{U}$ far from the bottom. For moderate currents[1] (time-averaged shear stress $\bar{\tau}$ smaller than $0.01\ \rho\ \hat{U}^2$) there exists a unique relation between $\hat{p}_b/\hat{U}$ and the ratio strokelength a (= $\hat{U}T/2\pi$ where T is the wave period) over bottom roughness r, which is shown in Figure 4 and can be approximated by:

$$\frac{\hat{p}_b}{\hat{U}} = \exp\left[\sum_{n=0}^{3} k_n \{\ln (a/r)\}^n\right] \tag{7}$$

wherein: $k_o = -1.092$; $k_1 = -.3364$; $k_2 = +.01876$; $k_3 = -4.621.10^{-4}$
Using $\hat{p}_b$ as basis for mathematical modeling, Figure 5 represents a dimensionless plot of the amplitude and phase of the first harmonic of the defect velocity $\hat{u}_d^*$ (= $\hat{u}_d/\hat{p}_b$) as function of the dimensionless

1) For larger currents is referred to Appendix B.

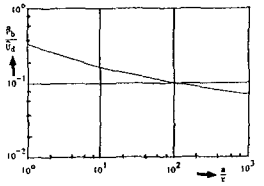

Figure 4 Relation between $\hat{p}_b/\hat{U}$ and a/r

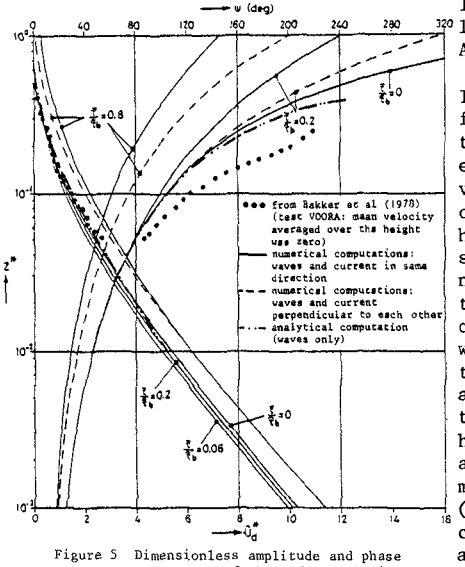

Figure 5 Dimensionless amplitude and phase of the defect velocity

height z^* above the bottom; here the height z above the bottom has been made dimensionless with a characteristic height Z, which refers to the intrusion depth of the instantaneous shear stresses i.e. the boundary layer thickness coherent with the oscillatory motion. Based on analytical considerations (see Appendix B) Z is expressed as:

$$Z = \kappa \hat{p}_b T \qquad (8)$$

In Figure 5 curves are given for waves and current codirectional and perpendicular to each other and for several values of mean shear stress over amplitude of the first harmonic of the bottom shear stress ($\bar{\tau}/\hat{\tau}_b$). The increasing numbers at the lines refer to these rates and give an increasing effect of current with respect to the oscillation. Here $\bar{\tau}$ denotes the time-averaged shear stress and $\hat{\tau}_b$ the amplitude of the first harmonic of the shear stress at the bottom. Increasing the mean shear stress results (after an initial small decrease) in an increase of the amplitude of the defect-velocity; for moderate currents ($\bar{\tau} < 0.01\ \rho\hat{U}^2$) the effect of magnitude and direction of the mean shear stress is small. The phase is more sensible for mean current changes. The dash-dot-lines in Figure 5 are the results of analytical computations, which are treated in Appendix B. For clearness' sake only the case without current is shown.

The dots in Figure 5 representing measurements of Bakker and Van Doorn show, that although the amplitude is rather well produced, the phase of the calculated oscillatory motion still has discrepancies with respect to measurements, due to deficiencies of the Prandtl model.

3 Time-averaged velocity field

Consider the time-averaged velocity field. The equation of motion reads (see also Appendix A and B):

$$\frac{\partial \underline{u}}{\partial t} = -\frac{1}{\rho} \text{grad } P + \frac{1}{\rho}\frac{\partial \underline{\tau}}{\partial z} \qquad (9)$$

wherein: grad P = horizontal pressure gradient

Averaging over the wave period, the acceleration term cancels out. For a flow with confined depth h, the shear stress increases linearly with the depth. Furthermore, the mixing length l should be:

$$l = \kappa z \sqrt{(1-z/h)} \qquad (10)$$

From Eq. (9) and (10), for stationary flow a logarithmic velocity distribution would result. However, this distribution would be found also from the assumptions made in this paper: a mixing length κz and a uniform shear stress over the depth.

The period mean velocity field can be derived from the internal shear stress velocity p, and a given mean shear stress by using Eq. (5) and (6) time averaged.
If, for simplicity in the two-dimensional case, only the mean $\bar{p}$ and first harmonic $\hat{p}$ of the shear stress velocity are considered, the shear stress according to Eq. (5) equals (ω being the angular velocity):

$$\tau = \rho(\bar{p} + \hat{p} \sin \omega t) \left|\bar{p} + \hat{p} \sin \omega t\right| \qquad (11)$$

Hence $\bar{\tau}$ is larger than $\rho \bar{p}^2$.

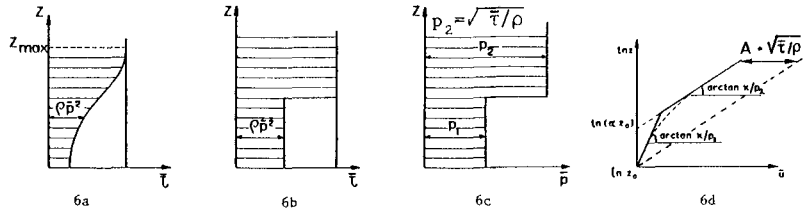

Figure 6 Computation mean velocity schematically

The nearer to the bottom, the larger the fluctuations of the shear stress and therefore, the larger the contribution of these fluctuations to the total shear stress. Thus the hatched part in Figure 6a shows the contribution of the mean shear stress velocity to the shear stress and the blank part the contribution of the variable part. One may schematize this picture to Figure 6b. The same figure is depicted in Figure 6c, however now the time-averaged shear stress velocity $\bar{p}$ is plotted on the horizontal axis instead of the mean shear stress $\bar{\tau}$.
The time averaged velocity can be found from integration the time-averaged Eq. (6) over the depth:

$$\bar{u} = \int_{z_o}^{z} \frac{\bar{p}}{\kappa z}\, dz \qquad \text{wherein: } z_o = r/33 \qquad (12)$$

Thus integrating Figure 6c over the depth, on logarithmic paper a broken line will come to being. This is shown schematically in Figure 6d. The gradient on the upper part is the same as one would have had without the effect of waves, but with the same pressure gradient (i.e. $\bar{\tau}$).
In fact, the lower part of the line in Figure 6d is not too important. One might extend the upper part in downward direction, thus finding an increase of the apparent roughness with a factor α. Lundgren (1972) presents this feature in the following way:

$$\bar{u}(z) = \sqrt{\bar{\tau}/\rho}\,\left(\frac{1}{\kappa} \ln \frac{z}{z_o} - A\right) \qquad (13) \quad \text{wherein:} \quad A = \frac{1}{\kappa} \ln \alpha \qquad (14)$$

In Eq. (13), $\bar{\tau}$ can be found from the waterlevel gradient [1]. This parameter A implies a reduction of the velocity u with A times the shear stress velocity (see Fig. 6d). The same is found for the depth-averaged velocity, as A does not depend on the level z.
For example: if the mean velocity is 1 m/s, corresponding with a shear stress velocity of 4 cm/s, a value A of 1 corresponds with a velocity reduction of 4 cm/s.

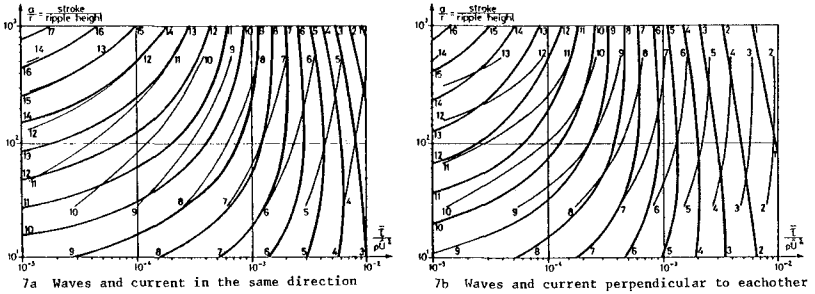

7a Waves and current in the same direction

7b Waves and current perpendicular to eachother

Figure 7 Comparison A-values according to Lundgren (1972) and analytical theory

In Figure 7 the values of A are plotted as function of $\bar{\tau}/(\rho \hat{U}^2)$ and a/r. Figure 7a shows the case, that waves and currents are codirectional, Figure 7b that waves and currents are perpendicular to each other. The thin lines refer to Lundgren (1972), the thick lines to the present theory. Differences in A between both theories are not more than 2 in the relevant area.
When waves and current are perpendicular to each other, the variations of p during the wave period are less than when waves and current are in the same direction. Thus $\rho\hat{p}^2$ will differ less from $\bar{\tau}$ (Fig. 6a) and therefore in the first case the factor A will be smaller (Fig. 7).
If one wants to implement the friction factors in a mathematical model, the use of graphs is inconvenient. For this goal the following formula for A may be useful:

$$A = \frac{1}{\kappa} (K_1 - K_2 \ln z_0^* + K_3 z_0^*) \qquad (15)$$

where K_1, K_2 and K_3 are given functions (see (C7)) of the ratio $\bar{\tau}/(\rho \hat{p}_b^2)$; the ratio $\hat{p}_b/\hat{U}$ is found from Eq. (7). The constants K_1, K_2 and K_3 also depend on the angle α_{wc} between waves and currents (appendix C). Furthermore , A is a function of the dimensionless z_0^* given in Eq.(C8) where z_0 (equal to r / 33) has been made dimensionless with the reference height Z (see Eq. (8)). Analytical calculations concerning A and the constants K_1, K_2 and K_3 are given in Appendix C.

1) In the case of breaking waves from the onshore gradient of the "shear stress" component of the radiation stress.

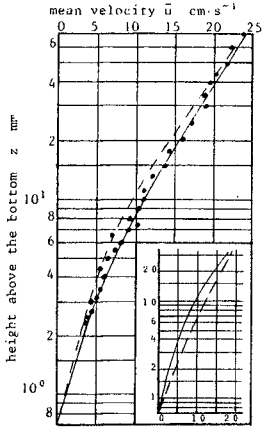

Figure 8 Mean velocity; theory compared with experiment of Bakker and Van Doorn (1978)

Figure 8 shows the velocity profile as result of measurements (Bakker and Van Doorn, 1978) and computations in a two-dimensional case.
The inset shows the same velocity profile again, in combination with the case that waves and current are perpendicular to each other. One observes, that the apparent roughness in the case with waves and current perpendicular to each other is smaller than for parallel wave- and current direction; for this extend the upper part of the lines in the inset in downward direction.

N.B. When using Eq. (13) for cases with combined waves and currents, it should be kept in mind, that the non-linear transport of water in the area above the wave trough falls outside the scope of this paper. This transport can be considerable.

4 Coastal engineering history

Very schematically, the history of science about the combination of waves and currents is the following (see Fig. 9).
In the past one did not realize oneself, that waves additional to current effect this current (Fig. 9a).
In 1967 for a given discharge Bijker pointed out the increase of shear stress by waves (Fig. 9b).
This inversely includes the reduction of current by waves, given a mean water level gradient.
In present time we realize ourselves, that waves change the vertical velocity distribution and therefore, that the reduction in discharge is not as drastically as Bijker predicts (Fig. 9c).

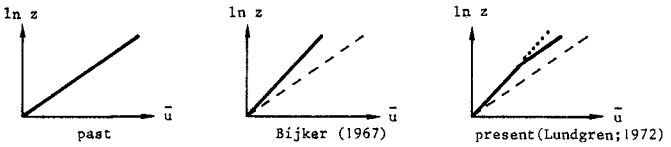

Figure 9 History of computation of mean velocity

5 Notation

a	strokelength ($=\hat{U}T/2\pi$)	(m)
A	factor determining the influence of waves on the time-averaged velocity-profile according to Lundgren (Eq.(13))	(-)
A, B	complex constants in hypergeometric functions (Eq.(B16))	(-)
a,b,c,d	constants in approximation K(z) (Eq.(B12) and (B13))	(-)
$C_{1,2,3,4}$	complex integration constants in Eq. (B16) to (B18)	(-)
E	complete elliptic integral of the second kind	(-)
$k_{i=0,1...}$	coefficient of power-series-expansions	(-)
$\text{ker}_i, \text{kei}_i$ $\text{ber}_i, \text{bei}_i$	Kelvin functions of order i	(-)
K	complete elliptic integral of the first kind	(-)
$K_{1,2,3}$	coefficients in Eq. (15) for A - value of Lundgren	(-)
$K(z)$	coefficient in differential equation analytical theory (Eq. (B4) and (B5))	(m^2s^{-1})
l	turbulent mixing length (Eq.(10))	(m)
m,n	constants in approximation influence α_{wc} on A-value Lundgren (Eq.(C2))	(-)
N_0, ϕ_0	modulus and phase of zero order Kelvin functions	(-)
p	internal shear stress velocity	(ms^{-1})
P	internal fluid pressure	(Pa)
r	Nikuradse roughness	(m)
$\underline{\underline{S}}$	second order tensor (Eq.(A9))	(-)
T	wave period	(s)
t	time	(s)
u	horizontal velocity	(ms^{-1})
U	horizontal velocity far from the bottom and boundary condition for the velocity field	(ms^{-1})
u_d	defect-velocity ($=u-U$; see also Fig. A1)	(ms^{-1})
x,y	horizontal coordinates	(m)
z	vertical coordinate	(m)
z_0	height above the bottom where the horizontal velocity is zero ($=r/33$)	(m)
Z	reference height for the boundary layer thickness coherent with the oscillatory motion (Eq.(8))	(m)
α	factor determining the increase of apparent bottom roughness (Eq.(14))	(-)
α_{wc}	angle between wave-propagation and current far from bottom	(deg)
β	tangent modulus in approximation of p^*	(-)
γ	Euler's constant	(-)
δ	direction of first derivative of horizontal velocity	(deg)
ζ	argument in analytical solution (Eq.(B16)	(-)
θ	phase of u_d (Eq.(B19))	(rad)
κ	Von Karman's constant	(-)
Λ	sum of digamma functions (Eq.(B16))	(-)
ν	kinematic viscosity	(m^2s^{-1})
ν_t	turbulent viscosity	(m^2s^{-1})
ξ	factor for influence α_{wc} in analytical theory (Eq.(B11))	(-)
ρ	specific density	(kgm^{-3})
τ	internal shear stress	(Pa)
ϕ	phase of $\tilde{p}$ (Eq.(B2))	(rad)
$\chi_{1,2}$	hypergeometric functions (Eq.(B16)	(-)
ψ	digamma function	(-)
ω	angular velocity ($2\pi/T$)	(s^{-1})

Other symbols added to a variable x:

$\underline{x}$	vector
x^*	dimensionless value
$\bar{x}$	time-averaged value
$\hat{x}$	amplitude first harmonic
$\tilde{x}$	first harmonic
x_b	value at the bottom

6 References

Bakker, W.T., 1973
Bottom friction and velocity distribution in an oscillatory flow,
Memo 72-23, Rijkswaterstaat, Directorate for Watermanagement and Hydraulic Research,
Department for Coastal Research.

Bakker, W.T. and Van Doorn, Th., 1978
Near bottom velocities in waves with a current,
Proc. 16th. Int. Conf. on Coastal Eng. Hamburg, ASCE, vol. II, pp. 1394-1414 (also: Publication 208,
Delft Hydraulics Laboratory, Delft, The Netherlands).

Bijker, E.W., 1967
Some considerations about scales for coastal models with movable bed,
Doctorate Dissertation, Delft University of Technology (also: Publication 50,
Delft Hydraulics Laboratory, Delft, The Netherlands).

Lundgren, H., 1972
Turbulent currents in the presence of waves,
Proc. 13th. Int. Conf. on Coastal Eng. Vancouver, ASCE, vol. II, pp. 623-634.

Appendix A: Numerical computations

Assumptions:

a. Only horizontal velocities, uniform in horizontal direction, are considered i.e. pressure gradient grad P uniform in vertical direction

b. The shear stress $\underline{\tau}$ can be found from the Prandtl hypothesis:

$$\underline{\tau} = \rho\, \nu_t \frac{\partial \underline{u}}{\partial z} \qquad \text{(A1)}$$

$$\nu_t = \kappa^2 z^2 \left|\frac{\partial \underline{u}}{\partial z}\right| \qquad \text{(A2)}$$

wherein:

$$\left|\frac{\partial \underline{u}}{\partial z}\right| = \sqrt{\left(\frac{\partial u_x}{\partial z}\right)^2 + \left(\frac{\partial u_y}{\partial z}\right)^2} \qquad \text{(A3)}$$

c. The time averaged shear stress $\overline{\tau}$ is uniform in vertical direction (cf ch.3).

Derivation of Eq. (1) and numerical solution:

According to assumption a the equation of motion reads:

$$\frac{\partial \underline{u}}{\partial t} = -\frac{1}{\rho} \text{grad } P + \frac{1}{\rho} \frac{\partial \underline{\tau}}{\partial z} \qquad \text{(A4)}$$

Define $\underline{U}$ and $\underline{u}_d$ in the following way:

$$\frac{\partial \underline{U}}{\partial t} = -\frac{1}{\rho} \text{grad } P \qquad \text{(A5)} \qquad \underline{u}_d = \underline{u} - \underline{U} \qquad \text{(A6)}$$

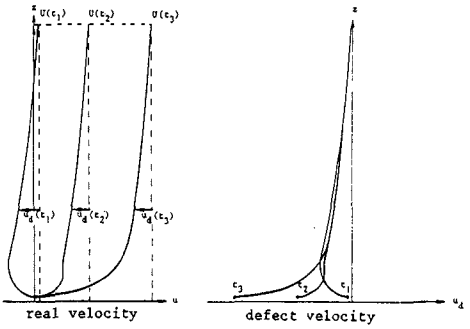

Figure A.1 Definition defect-velocity

The velocity $\underline{U}$ (only a function of t, cf. assumption a) denotes the velocity at a depth, to be chosen arbitrary, however far enough above the bottom to attenuate the periodical changes of $\underline{\tau}$. This can be seen from Eq. (A4) by taking the 2nd term on the right handside equal to zero (assumption c). The velocity $\underline{u}_d$ denotes the defect-velocity (see Fig. A1).

Substitution of Eq. (A5) and (A6) into (A4) yields:

$$\frac{\partial \underline{u}_d}{\partial t} = \frac{1}{\rho} \frac{\partial \underline{\tau}}{\partial z} \qquad \text{(A7)}$$

Write $\underline{\tau}$ as (τ_x, τ_y), and $\underline{u}$ as (u_x, u_y), then differentiation of τ_x to t gives, using Eq. (A1) to (A3):

$$\frac{\partial \tau_x}{\partial t} = \rho \left\{ \frac{\partial \nu_t}{\partial t} \frac{\partial u_x}{\partial z} + \nu_t \frac{\partial^2 u_x}{\partial t \partial z} \right\}$$

$$= \rho\, \nu_t \left\{ (1 + \cos^2 \delta) \frac{\partial^2 u_x}{\partial z \partial t} + \sin \delta \cos \delta \frac{\partial^2 u_y}{\partial z \partial t} \right\}$$

wherein: $\cos\delta = \frac{\partial \underline{u}_x}{\partial z} / \left|\frac{\partial \underline{u}}{\partial z}\right|$ and $\sin\delta = \frac{\partial \underline{u}_y}{\partial z} / \left|\frac{\partial \underline{u}}{\partial z}\right|$

Computation of $\partial\tau_y/\partial t$ in a similar way yields:

$$\frac{\partial \underline{\tau}}{\partial t} = \rho\, \nu_t\, \underline{\underline{S}}\, \frac{\partial^2 \underline{u}}{\partial z \partial t} \tag{A8}$$

wherein:
$$\underline{\underline{S}} = \begin{vmatrix} 1 + \cos^2\delta & \cos\delta \sin\delta \\ \cos\delta \sin\delta & 1 + \sin^2\delta \end{vmatrix} \tag{A9}$$

Differentiation of Eq. (A7) to z, multiplication with $\nu_t \underline{\underline{S}}$ and substitution of Eq. (A8) results in Eq. (1), because $\partial \underline{u}/\partial z$ equals $\partial \underline{u}_d/\partial z$.

With a similar derivation as the one for $\partial\underline{\tau}/\partial t$ one finds:

$$\frac{\partial \underline{\tau}}{\partial z} = \frac{\rho}{\kappa z}\, \nu_t\, \underline{\underline{S}}\, \frac{\partial}{\partial z} \left\{\kappa z \frac{\partial \underline{u}}{\partial z}\right\} \tag{A10}$$

Substitution of Eq. (A2) into (A10) and Eq.(A10) into (A7) yields an equation for the defect-velocity:

$$\frac{\partial \underline{u}_d}{\partial t} = \kappa z \frac{\partial \underline{u}_d}{\partial z} \cdot \underline{\underline{S}}\, \frac{\partial}{\partial z} \left\{\kappa z \frac{\partial \underline{u}_d}{\partial z}\right\} \tag{A11}$$

Eq. (A11) has been solved numerically using a finite difference method based on the Crank-Nicholson implicite integration scheme with the boundary conditions:

$\underline{u}_d = \underline{0}$ at the upper end
$\underline{u}_d = -\underline{U}$ near the bottom at a height z_o which is proportional to the dimension of the bottom roughness r (z_o = r/33)
$\underline{U}$ = imposed velocity at the upper boundary

Appendix B: Analytical computations

In this appendix only relations will be derived, on one hand for parallel direction of oscillation and current (i.e. $\alpha_{wc} = 0°$) and on the other hand for oscillation and current perpendicular to each other (i.e. $\alpha_{wc} = 90°$).
Differentiation of the equation of motion (A4) to z using assumption a, multiplication with κz and substitution of (6) gives:

$$\frac{\partial \underline{p}}{\partial t} = \frac{1}{\rho} \kappa z \frac{\partial^2 \underline{\tau}}{\partial z^2} \tag{B1}$$

When only the first harmonics are taken into account for the linearized approximation the shear stress $\underline{\tau}$ and shear stress velocity $\underline{p}$ can be written as:

$$\begin{aligned} \underline{p} &= \overline{\underline{p}} + \tilde{\underline{p}}\,; \qquad \tilde{\underline{p}} = \hat{\underline{p}} \sin(\omega t + \phi) \\ \underline{\tau} &= \overline{\underline{\tau}} + \tilde{\underline{\tau}}\,; \qquad \tilde{\underline{\tau}} = \hat{\underline{\tau}} \sin(\omega t + \phi) \end{aligned} \tag{B2}$$

wherein: ϕ = phase of $\tilde{\underline{p}}$ and equals in an approximation upto the first harmonic the phase of $\tilde{\underline{\tau}}$

Because $\tilde{\underline{p}}$ and $\tilde{\underline{\tau}}$ are in phase, derivation to t yields in the case of $\alpha_{wc} = 0°$ and 90°:

$$\frac{\partial \tilde{\underline{p}}}{\partial t} = \frac{\hat{p}}{\hat{\tau}} \cdot \frac{\partial \tilde{\underline{\tau}}}{\partial t} \qquad \text{(B3)}$$

wherein: $\hat{p}, \hat{\tau}$ the modulus of $\hat{\underline{p}}$ and $\hat{\underline{\tau}}$

Evidently Eq. (B3) is only relevant in the plane of oscillation. Only considering this plane in the following, the vector-sign (underlining) may be skipped.

After substitution of (B3) into (B1) and using assumption c an equation, similar to (1) is found[1]:

$$\frac{\partial \tilde{\tau}}{\partial t} = K \frac{\partial^2 \tilde{\tau}}{\partial z^2} \qquad \text{(B4)} \qquad \text{wherein: } K = \kappa z \frac{\hat{\tau}/\rho}{\hat{p}} \qquad \text{(B5)}$$

For $\alpha_{wc} = 0°$ from Eq. (5) and (B2) can be derived:

$$\frac{\hat{\tau}}{\rho \hat{p}^2} = \frac{4}{\pi} \frac{\bar{p}}{\hat{p}} \arcsin \frac{\bar{p}}{\hat{p}} + \frac{4}{3\pi} \left(2 + \frac{\bar{p}^2}{\hat{p}^2}\right) \sqrt{1 - \frac{\bar{p}^2}{\hat{p}^2}} \quad \text{for } \bar{p} < \hat{p}$$

$$\frac{\hat{\tau}}{\rho \hat{p}^2} = 2 \bar{p}/\hat{p} \quad \text{for } \bar{p} > \hat{p} \qquad \text{(B6)}$$

$$\frac{\bar{\tau}}{\rho \hat{p}^2} = \frac{2}{\pi} \left(\tfrac{1}{2} + \frac{\bar{p}^2}{\hat{p}^2}\right) \arcsin \frac{\bar{p}}{\hat{p}} + \frac{3}{\pi} \frac{\bar{p}}{\hat{p}} \sqrt{1 - \frac{\bar{p}^2}{\hat{p}^2}} \quad \text{for } \bar{p} < \hat{p}$$

$$\frac{\bar{\tau}}{\rho \hat{p}^2} = \tfrac{1}{2} + \frac{\bar{p}^2}{\hat{p}^2} \quad \text{for } \bar{p} > \hat{p} \qquad \text{(B7)}$$

These keep their validity in dimensionless shape, wherein $\bar{p}$, $\hat{p}$, $\bar{\tau}$ and $\hat{\tau}$ are made dimensionless with the value of $\hat{p}$ at the bottom (i.e. $\hat{p}_b$ for $\bar{p}$ and $\hat{p}$, and $\rho \hat{p}_b^2$ for $\bar{\tau}$ and $\hat{\tau}$). In the following these dimensionless values are denoted with an asterisk.

1) Eq. (B4) is quite similar to (1). Generally it should be kept in mind, that Eq. (B4) is a linearized equation, where (1) has general validity, and therefore the coefficient K is not equal to ν_t [2]. However for parallel oscillation and current δ equals 0, and therefore in the plane of oscillation Eq. (1) and (A9) yields:

$$\frac{\partial \tau}{\partial t} = 2 \nu_t \frac{\partial^2 \tau}{\partial z^2} \qquad \text{wherein: } \nu_t = \kappa^2 z^2 \left| \frac{\partial u}{\partial z} \right|$$

For large z the value of $|\partial u/\partial z|$ approaches $\bar{p}/\kappa z$, and therefore $2\nu_t \to 2 \kappa z \bar{p}$. As $\hat{\tau}/\rho$ will be $2 \bar{p}\hat{p}$ for large value of z (see Eq. (B6)), the value of K according to Eq. (B5) equals $2 \nu_t$. This demonstrates the similarity between Eq. (1) and (B4) in this case.

2) Even, generally, the time-independent K is not equal to the time-averaged $\underline{\underline{S}}\ \nu_t$.

In Figure B1 is displayed a dimensionless $K^* = K/(\kappa^2 \hat{p}_b^2 T)$ versus a dimensionless height $z^* = z/(\kappa_b \hat{p} T)$.
Furthermore the value of K^* depends on $\bar{\tau}/\hat{\tau}_b$. For the relation $\hat{p}^* = \hat{p}/\hat{p}_b$ an exponential decay is assumed (Bakker, 1973):

$$\hat{p}^* = e^{-(3\pi^3/16)\, z^*} \tag{B8}$$

The rate of decay according to Eq. (B8) is coherent with the choice of the reference height Z, defined as $Z = \kappa \hat{p}_b T$.
A relation between $\bar{\tau}^*/\hat{\tau}_b^*$ and $\bar{p}_b^*$ follows from division of (B7) by (B6). Given the value of $\bar{\tau}^*/\hat{\tau}_b^*$ using Eq. (B8) the value of $\bar{p}_b^*$ can be found. From (B7) results $\bar{\tau}^*$. For a certain level z^*, the value of $\hat{p}^*$ follows from Eq. (B8). As $\bar{\tau}^*$ remains constant in the vertical sense, the value of $\bar{\tau}^*/\hat{p}^{*2}$ is known. Substitution of this value in Eq. (B7) yields a value of $\bar{p}^*/\hat{p}^*$, which further can be substituted in Eq. (B6) yielding $\tau^*/\hat{p}^{*2}$ and therefore K^* $(= z^* \hat{\tau}^*/\hat{p}^*)$
For $\alpha_{wc} = 90°$ a similar approach can be chosen. Instead of Eq. (B6) and (B7) is found:

$$\frac{\hat{\tau}}{\rho \hat{p}^2} = \frac{4}{3\pi}\sqrt{1+\frac{\bar{p}^2}{\hat{p}^2}}\left[(2+\frac{\bar{p}^2}{\hat{p}^2})E\{\frac{1}{1+\bar{p}^2/\hat{p}^2}\} - \frac{\bar{p}^2}{\hat{p}^2} K\{\frac{1}{1+\bar{p}^2/\hat{p}^2}\}\right] \quad \text{for } \bar{p}/\hat{p} > 0 \tag{B9}$$

$$\frac{\bar{\tau}}{\rho \hat{p}^2} = \frac{2}{\pi}\frac{\bar{p}}{\hat{p}}\sqrt{1+\frac{\bar{p}^2}{\hat{p}^2}}\; E\{\frac{1}{1+\bar{p}^2/\hat{p}^2}\} \quad \text{for } \bar{p}/\hat{p} > 0 \tag{B10}$$

wherein: $K\{\}$ = complete elliptic integral of the first kind
$E\{\}$ = complete elliptic integral of the second kind

For the analytical computations of the time-dependent velocity field the coefficient K^* is approximated in 3 sections (see Fig. B1):
Above the intersection of the straight line and the curve valid for waves only, the straight line is assumed i.e.:

$$\text{upper part: } K^* = \xi . z^* \sqrt{\bar{\tau}^*} \tag{B11}$$

wherein: $\xi = 2$ for $\alpha_{wc} = 0°$;
$\xi = 1$ for $\alpha_{wc} = 90°$

Eq. (B11) follows from substitution of Eq. (B6) ($\alpha_{wc} = 0°$) or Eq. (B9) ($\alpha_{wc} = 90°$) into Eq. (B5) for the limiting case of $\bar{p}/\hat{p} \to 0$ and $\bar{p} \to \sqrt{\bar{\tau}/\rho}$.
Below the intersection of the straight line and the curve for waves only, the curve is assumed, which is approximated by:

$$\text{middle part: } K^* = a e^{-bz^*} \quad ; a = 0.111 \quad b = 3.267 \tag{B12}$$

$$\text{lower part: } K^* = cz^* - dz^{*2} \quad ; c = 0.849 \quad d = 2.817 \tag{B13}$$

The intersection of lower and middle part is situated at $z^* = 0.186$.
The influence of the current on the time-dependent solution is restricted to the upper part where Eq. (B11) is valid. As long as the straight line in Figure B1 intersects the curve I + II for waves only, the influence of the current on the time-dependent velocity field is negligible near the bottom. This can also be seen from nu-

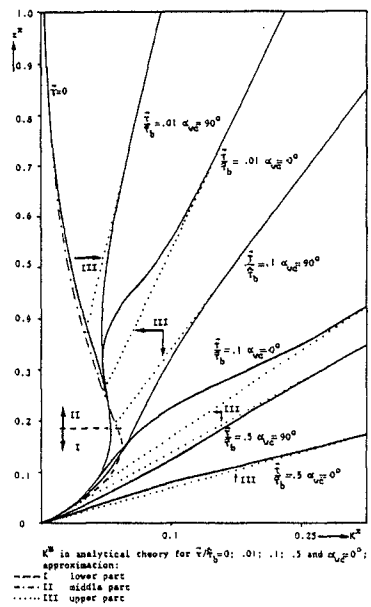

Figure B.1 Coefficient K^* as function of z^* (analytically and approximation)

merical computations in Figure 5.[1] The intersection disappears for large currents, when the slope of the straight line exceeds the tangent of the basic curve at the origin (Fig. B1) i.e.:

$$\xi \sqrt{\tilde{\tau}^*} > \frac{8}{3\pi} \qquad \text{(B14)}$$

With above given approximations for K^*, Eq. (B4) can be solved analytically with the boundary conditions:

$$\begin{aligned} z = 0: \ & \underline{\tau} = \overline{\tau} + \hat{\tau}_b \sin \omega t \\ z \to \infty: \ & \underline{\tau} \to \overline{\tau} \end{aligned} \qquad \text{(B15)}$$

When the time dependent shear stress $\tilde{\tau}$ is found, with Eq. (A7) the time-dependent defect velocity $\tilde{u}_d$ can be computed. The analytical solutions for the amplitude and phase of the first harmonic of u_d (in complex form; suffix c denotes 'complex') are determined apart from complex integration constants C_1, C_2, C_3 en C_4:

lower part: the solution consists of hypergeometric functions, which in the following already are expressed in power-series-expansions

$$\hat{u}^*_{dc} = \frac{d}{\kappa c}\left[C_1\{1 + \chi_1(\zeta)\} + \frac{\hat{\tau}^*_b}{d}\{1 + \ln \zeta + \chi_2(\zeta)\}\right] \qquad \text{(B16)}$$

wherein: c,d are given in Eq. (B13)

$$\chi_1(\zeta) = \sum_{n=1}^{\infty} \frac{(A+1)_n (B+1)_n}{(n+1)!\ n!} \cdot n \cdot \zeta^{n-1}$$

$$\chi_2(\zeta) = \sum_{n=1}^{\infty} \frac{(A+1)_n (B+1)_n}{(n+1)!\ n!} \cdot n \cdot \zeta^{n-1} \Lambda(n)$$

$$(A+1)_n = (A+1)\ (A+2)\ \ldots\ldots\ (A+n)$$

$$\Lambda(n) = \psi(A+1+n) - \psi(A+1) + \psi(B+1+n) - \psi(B+1) - \psi(n+2) + \psi(2) - \psi(n+1) + \psi(1)$$

$$\psi(m) = \text{digamma function} = -\gamma + \sum_{n=1}^{m-1} \frac{1}{n}$$

1) Mind that (exact) the same solution is found for waves and current codirectional and perpendicular to each other, if in the last case the time-averaged shear stress is four times as large as in the first case (because then part III is the same; see Eq. (B11)).

γ = .57722 (Euler's constant)
A,B = complex constants restricted by
A + B = -1; A.B = $2\pi i/d$
(as d = 2.817: A = 0.617 - 0.999 i
B = -1.617 + 0.999 i)
$\zeta = \frac{d}{c} \cdot z^*$

middle part: the solution consists of Kelvin functions:

$$\hat{u}^*_{dc} = \frac{b\,\zeta}{\kappa}\left[C_2\{\mathrm{ker}_1(\zeta) + i.\mathrm{kei}_1(\zeta)\} + C_3\{\mathrm{ber}_1(\zeta) + i.\mathrm{bei}_1(\zeta)\}\right] \quad \text{(B17)}$$

wherein: $\zeta = 2\pi\sqrt{\frac{2}{\pi a}}\, e^{\frac{1}{4}bz^*}$

$\mathrm{ker}_1(\zeta)$, $\mathrm{kei}_1(\zeta)$, $\mathrm{ber}_1(\zeta)$ and $\mathrm{bei}_1(\zeta)$ are Kelvin functions
upper part:

$$\hat{u}^*_{dc} = C_4\left[\mathrm{ker}_o(\zeta) + \mathrm{kei}_o(\zeta) + i\{\mathrm{kei}_o(\zeta) - \mathrm{ker}_o(\zeta)\}\right] \quad \text{(B18)}$$

wherein: $\zeta = 2\sqrt{\frac{2\pi z^*}{\xi\sqrt{\bar{\tau}^*}}}$

For large currents, when only the upper part can be applied, Eq. (B18) becomes:

$$\hat{u}^*_d = \frac{2\hat{\tau}^*_b}{\xi\sqrt{\bar{\tau}^*}} \cdot \frac{1}{\kappa} N_o(\zeta) \quad ; \quad \theta = \Phi_o(\zeta) \quad \text{(B19)}$$

wherein: $N_o(\zeta) = \sqrt{\mathrm{ker}_o^2(\zeta) + \mathrm{kei}_o^2(\zeta)}$
$\Phi_o(\zeta)$ = arctan $\{\mathrm{kei}_o(\zeta)/\mathrm{ker}_o(\zeta)\}$
θ_o = phase of $\tilde{u}_d$ defined by $\hat{u}_d = \hat{u}_d \sin(\omega t+\theta)$

For clearness' sake only the analytical solution for the case of waves only is presented in Figure 5. The analytical solution then consists only of the combination of Eq. (B16) and (B17).

From Eq. (B19) a simple relation can be derived between the ratio $\hat{\tau}_b/(\rho\hat{U}^2)$ and the ratio strokelength over bottomroughness a/r. Replace in Eq. (B19) the dimension operator $\hat{p}_b$ (denoted by a asterisk) by $\hat{U}$, and consider Eq. (B19) at a level $z=z_o$, where $\hat{u}_d = \hat{U}$. The result is:

$$\frac{\hat{\tau}_b}{\rho\hat{U}^2} = \frac{\kappa\,\xi}{2}\sqrt{\frac{\bar{\tau}}{\rho\hat{U}^2}}\; N_o^{-1}(\zeta) \quad \text{(B20)}$$

wherein: $\zeta = \dfrac{2}{\sqrt{33\ \kappa\xi\ a/r\ \sqrt{\bar{\tau}/\rho\hat{U}^2}}}$

This equation is only valid when Eq. (B14) can be applied. Practically Eq. (B19) and (B20) differ only slightly from the numerical solution in the range of $a/r > 1$ and $\bar{\tau}/(\rho\,\hat{U}^2) \gg 0.1$.

Appendix C: Analytical calculation of Lundgren's A-value

In this appendix the analytical solution for the time-averaged velocity field will be treated. With Eq. (12) this field can be found from the time-averaged shear stress velocity. The last can be found from the definition of the shear stress velocity by Eq. (5) in the following way[1)]

As described in Appendix B, the ratio $\bar{p}^*/\hat{p}^*$ [2)] can be found as function of the dimensionless height z^* above the bottom using Eq. (B7) when $\alpha_{wc} = 0°$ and Eq. (B10) when $\alpha_{wc} = 90°$. From Eq. (B8) the dimensionless $\bar{p}^*$ can be derived. For various values of $\bar{\tau}/\hat{\tau}_b$ those curves are plotted in Figure C1, in the case of $\alpha_{wc} = 0°$.

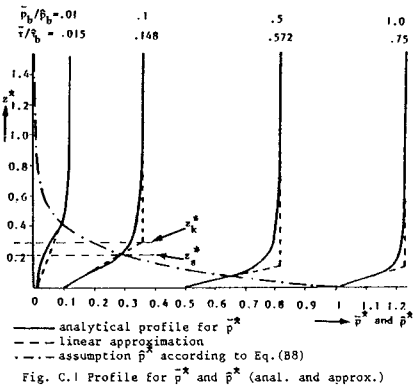

Fig. C.1 Profile for $\bar{p}^*$ and $\hat{p}^*$ (anal. and approx.)

For integrating over the depth according to Eq. (12) the curves for $\bar{p}^*$ are approximated by a vertical and an oblique line (see Fig. C1). The vertical line corresponds with the value of $\bar{p}^* = \sqrt{\bar{\tau}^*}$, the oblique line connects the bottom point $\bar{p}^* = \bar{p}_b^*$ with the point, where $\bar{p}^* = \hat{p}^*$:

$$\bar{p}^* = \bar{p}_b^* + \beta z^* \qquad \text{(C1)}$$

This approximation can only be applied, when $\bar{p}_b^* < 1$. As will be shown later this restriction covers the cases where the influence of waves on a current becomes significant. As the dash-dot line in Figure C1 denotes $\hat{p}^*$(given by Eq. (B8)), the intersection point of the drawn line and the dash-dot line is also a point of the oblique line.

From Eq. (B7) and (B10) it shows, that in the intersection points, $(z^* = z_s^*)$, where $\bar{p}^* = \hat{p}^*$ the value of $\bar{\tau}^* / \hat{p}^{*2}$ equals 1.5, when $\alpha_{wc} = 0°$ and $2\sqrt{2}/\pi\ E\{\frac{1}{2}\} \simeq 1.216$ when $\alpha_{wc} = 90°$C. Generally it can be derived that:

$$\hat{p}^* = \sqrt{\frac{\bar{\tau}^*}{1 + (m + n \cos^2 \alpha_{wc})^2}} \qquad \text{(C2)}$$

wherein: $m^2 = \frac{2\sqrt{2}}{\pi} E\{\tfrac{1}{2}\} - 1 \simeq 0.216$

$n = \frac{1}{2}\sqrt{2} - m$

$E\{\}$ = complete elliptic integral of the second kind.

Using Eq. (B8) for $\hat{p}^*$ from Eq. (C1) the height of the intersection level $z^* = z_s^*$ is found:

$$z_s^* = -\frac{8}{3\pi^3} \ln\left\{\frac{\bar{\tau}^*}{1 + (m + n \cos^2 \alpha_{wc})^2}\right\} \qquad \text{(C3)}$$

1) In an approximation, up to the first harmonic.
2) The asterisks have the same meaning as in Appendix B.

Then from Eq. (C1) β can be derived:

$$\beta = (\hat{p}^* - \bar{p}_b^*)/z_s^* \tag{C4}$$

The level z_k^*, where the vertical line and the oblique line intersect equals:

$$z_k^* = (\sqrt{\bar{\tau}^*} - \bar{p}_b^*)/\beta \tag{C5}$$

From integration, according to Eq. (12), the velocity $\bar{u}_k^*$ at the level z_k^* can be found. For $z^* > z_k^*$ a logarithmic velocity profile is found (Fig. 6d) i.e. a straight line on logarithmic paper through the point $(z_k^*, \bar{u}_k^*)$ under the inclination arctan $(\kappa/\sqrt{\bar{\tau}/\rho})$. Extension of this line in downward direction yields the level αz where α is the magnification of the apparent bottom roughness (Fig. 6d):

$$\ln \alpha = \left(1 - \frac{\bar{p}_b^*}{\sqrt{\bar{\tau}^*}}\right) \ln \frac{z_k^*}{z_o^*} - \frac{\beta}{\sqrt{\bar{\tau}^*}} (z_k^* - z_o^*) \tag{C6}$$

Using Eq. (14) this gives the A-value of Lundgren according to Eq. (15) wherein:

$$K_1 = K_2 \ln z_k^* - K_3 z_k^* \; ; \; K_2 = 1 - \frac{\bar{p}_b^*}{\sqrt{\bar{\tau}^*}} \; ; \; K_3 = \frac{\beta}{\sqrt{\bar{\tau}^*}}$$

(β and z_k^* according to Eq. (C4) and (C5))
The coefficient K_1, K_2 and K_3 can be written as function of $\bar{\tau}/(\rho\, \hat{p}_b^{\,2})$ and α_{wc}. These functions are approximated with power-series-expansions for the cases $\alpha_{wc} = 0°$ and $\alpha_{wc} = 90°$:

$$K_i = \sum_{n=0}^{4} k_{in} \{\ln(\frac{\bar{\tau}}{\rho \hat{p}_b^2})\}^n (i = 1,2,3) \tag{C7}$$

The coefficients k_{in} are listed in the table below.

	$\alpha_{wc} = 0°$					$\alpha_{wc} = 90°$				
	k_0	k_1	k_2	k_3	k_4	k_0	k_1	k_2	k_3	k_4
K_1	-.914	.623	.159	.0110	-	-.3921	.2264	-.1325	-.0410	-.002850
K_2	.284	-.285	-.0416	-.00214	-	.1120	-.0858	.0737	.0175	.001092
K_3	2.654	-.511	-.408	-.0761	-.00464	1.3845	.1398	.3302	.0883	.006240

The values of the coefficients for $0° < \alpha_{wc} < 90°$ can be approximated by linear interpolation.
Eq. (C7) and (15) relate A to $\bar{\tau}/(\rho \hat{p}_b^2)$ and z_0^*; this relationship can be easily converted to the presentation according to Lundgren (Fig. 7). Here $\bar{\tau}/(\rho \hat{U}^2)$ replaces $\bar{\tau}/(\rho \hat{p}_b^2)$. Evidently these dimensionless variables can be converted to each other with the aid of the ratio $\hat{p}_b/\hat{U}$, given in Eq. (7) as function of the ratio a/r. Furthermore in Lundgren's presentation the variable a/r replaces z_0^*; these variables are related in the following way (using Eq. (8)):

$$z_0^* = \frac{z_0}{\kappa \hat{p}_b T} = \frac{1}{66\kappa\pi} \frac{\hat{U}}{\hat{p}_b} \frac{1}{a/r} \tag{C8}$$